Electronic Supplementary Information (ESI)

Low-Carbon Upcycling of Vanadium Slag into Doped Cathodes for High-performance Zinc Batteries

Lin Guo[a,b,c], Wenting Jia[a,b,c], Junmei Zha[a,b,c], Gaojie Xu[a,b,c], Pengge Ning[a,b,c,], Hongbin Cao[a,b,c,*]*

[a]Chemistry & Chemical Engineering Data Centre, National Engineering Research Centre of Green Recycling for Strategic Metal Resources, Chinese Academy of Sciences, Beijing 100190, P. R. China

[b]School of Chemical Engineering, University of Chinese Academy of Sciences, Beijing 100049, P. R. China

[c]Institute of Process Engineering, Chinese Academy of Sciences, Beijing 100190, P. R. China

*Corresponding authora:

Prof. Pengge Ning, Prof. Hongbin Cao

Institute of Process Engineering, Chinese Academy of Science, Beijing 100190, China

Email: pgning@ipe.ac.cn; hbcao@ipe.ac.cn

Keywords: short-process synthesis; doped vanadium-based cathodes; structural modification; synergistic effect; carbon emission reduction

Contents

Section S1. Experimental section

1.1 Preparation of materials

The sodium-roasted alkaline leachate of vanadium slag and its desilicated solution were obtained from Pangang Group Co, Ltd (Sichuan, China). The concentration ranges of the primary elements in the leachate are provided in Table S1. The desilication agent LK-SI reduces the silicon concentration in the leachate to below 20 mg L^{-1}, while the concentrations of other elements show minimal variation. The preparation steps for NHVO-M_x are as follows: 2.1 g of ammonium sulfate was added into 30 mL of simulated desilicated leachate, and the mixture was stirred continuously for 3 h. Afterward, the filtered precipitate was then calcined at 300 °C in a nitrogen atmosphere for 2 h, yielding vanadium oxide doped with various metal ions such as Cr, Si, Ca, and K, and intercalated with ammonium ions (NHVO-M_x). NHVO was prepared using a sodium metavanadate solution free of impurities, while NHVO-Cr, NHVO-Si, NHVO-Ca, and NHVO-K were synthesized using simulated leachates containing single impurities at different concentrations. These subsequent steps remained unchanged. Since the solutions used to prepare NHVO, NHVO-M_x, NHVO-Ca, NHVO-Cr, and NHVO-K all contain a significant amount of sodium ions, the sodium concentration in the solution after digesting and diluting 3 mg of samples to 100 mL ranges from 0.2 to 0.59 mg/L. As a result, all the samples contain sodium at similar concentrations. Therefore, we did not conduct a separate study on Na doping. To investigate the optimal calcination conditions, NHVO were synthesized at calcination temperatures of 250 °C, 300 °C, and 350 °C, with calcination times of 1.5 h, 2 h, and 3 h, while all other procedures remained unchanged.

1.2 Characterization

The material's structural and phase properties were analyzed using X-ray diffraction (Bruker) with Cu Kα radiation. Raman spectroscopy (Renishaw, in Via, England) was performed with a 532 nm wavelength laser. The band structure was obtained using a UV-VIS-NIR spectrophotometer (Agilent Cry 7000 series). The sample morphology was examined through field emission scanning electron microscopy (JSM-7800) and transmission electron microscopy (JEOL JEM-2100F). X-ray photoelectron spectroscopy (XPS) was carried out on a Thermo

ESCALAB 250Xi with Al Kα (1486.6 eV) radiation. The electron paramagnetic resonance (EPR) spectroscopy was carried out by Bruker Magnettech EPR5000 to detect the defect character. The concentration of metal ions was determined via ICP-OES (OPTIMA 6300DV, Perkin-Elmer, USA), with a calibration curve precision of 99.99%. The data were plotted using Origin Learning Edition, and the crystal structure diagrams were drawn using VESTA.

1.3 Electrochemical measurements

All electrochemical tests were conducted at room temperature. The active material, carbon black (Super P), and polyvinylidene fluoride (PVDF) binder were mixed in a weight ratio of 7:2:1 and dissolved in an appropriate amount of N-methyl-2-pyrrolidone (NMP) to form a homogeneous slurry. This slurry was then coated onto a 0.02 mm thick titanium foil and dried in a vacuum oven at 70 °C. The active material loading on each working electrode was approximately 1.5 mg cm^{-2}. Glass fiber (GF/D), 2M $Zn(CF_3SO_3)_2$ aqueous solution, and zinc foil (0.1 mm) were used as the separator, electrolyte, and anode, respectively. The components, along with the previously prepared cathode, were assembled into CR2032 coin cells for electrochemical testing. Galvanostatic charge/discharge measurements were conducted using the LAND-CT2001A at varying current densities within a voltage range of 0.2 to 1.6 V (vs. Zn^{2+}/Zn). The Galvanostatic Intermittent Titration Technique (GITT) was also performed on the LAND-CT2001A at 50 mA g^{-1}, with each discharge pulse lasting 10 minutes followed by a 30-minute relaxation period for each step. Cyclic voltammetry (CV) and electrochemical impedance spectroscopy (EIS) tests were carried out using an electrochemical workstation (CHI760D, Shanghai Chenhua).

The soft-packaged pouch cell was assembled with a cathode (6.5 cm × 8.0 cm) and a Zn anode (8.0 cm × 9.5 cm), separated by Glass fiber (GF/D) in 2M $Zn(CF_3SO_3)_2$ electrolyte. During assembly, the components were sealed within a soft pouch. The cathode foil was prepared by mixing active materials, carbon black, and PVDF binder in a weight ratio of 8:1:1 in NMP to form a slurry, which was then coated onto a titanium mesh. The coated mesh was dried at 70°C for over 12 hours. The loading of the active material was 21.9 mg cm^{-2}. Finally, the pouch cell was tested at room temperature to evaluate its capacity and stability.

1.4 Computational Methods

All calculations were performed with periodic DFT using the Gaussian plane wave method implemented in CP2K's Quickstep module[1,2]. The explorative studies of the catalysts structure were performed using the molecularly optimized basis set DZVP-MOLOPT-SR-GTH for each atom with a Goedecker-Teter-Hutter (GTH) pseudopotential[3]. The calculations were conducted using the generalized gradient approximation and the Perdew-Burke-Ernzerhof (PBE) functional with DFT-D3 correction[4,5]. An energy convergence for the self-consistent field (SCF) calculation was set to 5×10^{-6} Hartree. The 1×3×1 supercell was employed both in V_2O_5 and NHVO-M_x model. The k-points was set as 2×2×5. An energy cutoff of 400 Ry was used throughout the calculations. The input file was generated by Multiwfn[6].

1.5 Comprehensive environmental assessment

Comprehensive Environmental Assessment (CEA) was utilized to evaluate the environmental impact of emissions during production processes, employing the calculation methods outlined in previous studies of Gao et al[7]. In the process from leachate to vanadium products, solid waste was effectively treated and recycled; therefore, this aspect is not discussed further in the present study. Wastewater is the primary pollutant in this study, and the CEA is predominantly based on the assessment of wastewater. Since all three production processes involve an ammonium metavanadate precipitation step, the composition of wastewater from this stage is similar across the processes. Therefore, it is assumed that the environmental impact of this specific wastewater component is excluded from the comparative evaluation. The calculation of carbon emissions was based on the electricity and heat conversion factors from the "Norm of Energy Consumption per Unit Production of Coal to Olefins, Coal to Synthetic Natural Gas, and Coal to Liquids" - GB 230180-2024 (Chinese Standards and Regulations, 2024) and the carbon dioxide equivalent conversion from the "Requirements of Greenhouse Gas Emissions Accounting and Reporting - Part 10: Chemical Production Enterprise" - GB/T 32151.10-2015 (Chinese Standards and Regulations, 2015).

1.6 Economic assessment

The economic assessment of the production processes for vanadium-based cathode materials

was conducted using the method proposed by Gao et al[8]. This analysis considered the following parameters: 1. Macro costs: raw material cost C_{RM}, operating cost C_O, total cost C_T; 2. Process costs: pre-treatment cost C_{PT}, separation and purification cost C_{SP}, productization process cost C_P; waste treatment cost C_{WT} (*e.g.*, wastewater, waste gases, solid waste); 3. Various types of costs: water cost C_w (*e.g.*, water, steam), material cost C_m (*e.g.*, NaOH, H_2SO_4, $(NH_4)_2SO_4$), energy cost C_e (*e.g.*, electricity), auxiliary costs C_a(*e.g.*, packaging, labor, equipment depreciation), as well as costs from various components and other cost (*e.g.*, period cost, variable cost).

1.7 Data collection

To ensure the reliability of the assessment, raw data on materials, energy, water, and waste emissions were soured from both a representative enterprise in Panzhihua, Sichuan, China and actual experimental data. These data were then normalized. The analysis has certain limitations and scope. Cost and environmental impacts could vary depending on the choice of precipitants or extractants used in the process. Due to variations in regional processes and raw materials, results may differ in other regions. Differences in electricity prices across regions may also affect cost assessments. These variations can be reviewed through industrial raw material price websites (https://prices.sci99.com/). Unit prices for raw materials, energy, and water were derived from the average market prices in Panzhihua, Sichuan, China (the country's largest vanadium production base) between 2018 to 2024. The wastewater discharge standards were referenced from the "Discharge standard of pollutants for the vanadium industry" - GB 26452-2011 (Chinese National Standards and Regulations, 2011).

Section S2. Results and Discussion

2.1 Supplementary Figures

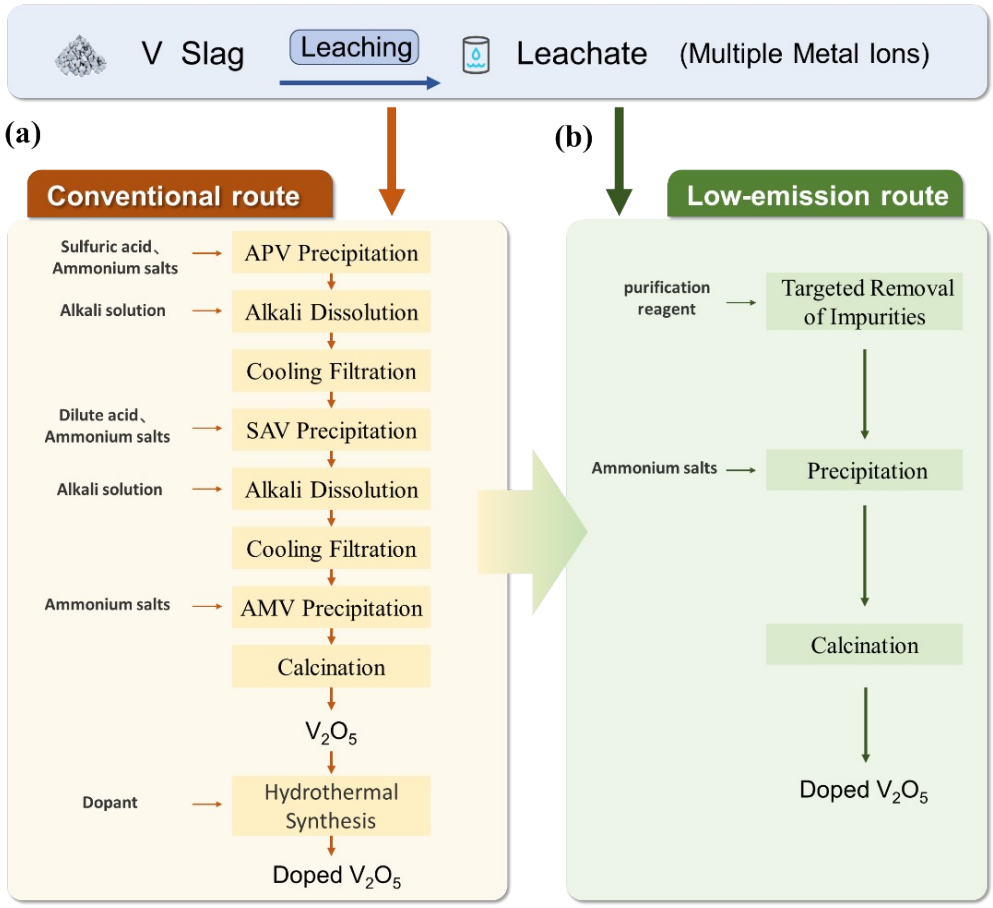

Fig. S1 Comparison of (a) common and (b) green synthesis routes for doped vanadium oxide and the reagents involved

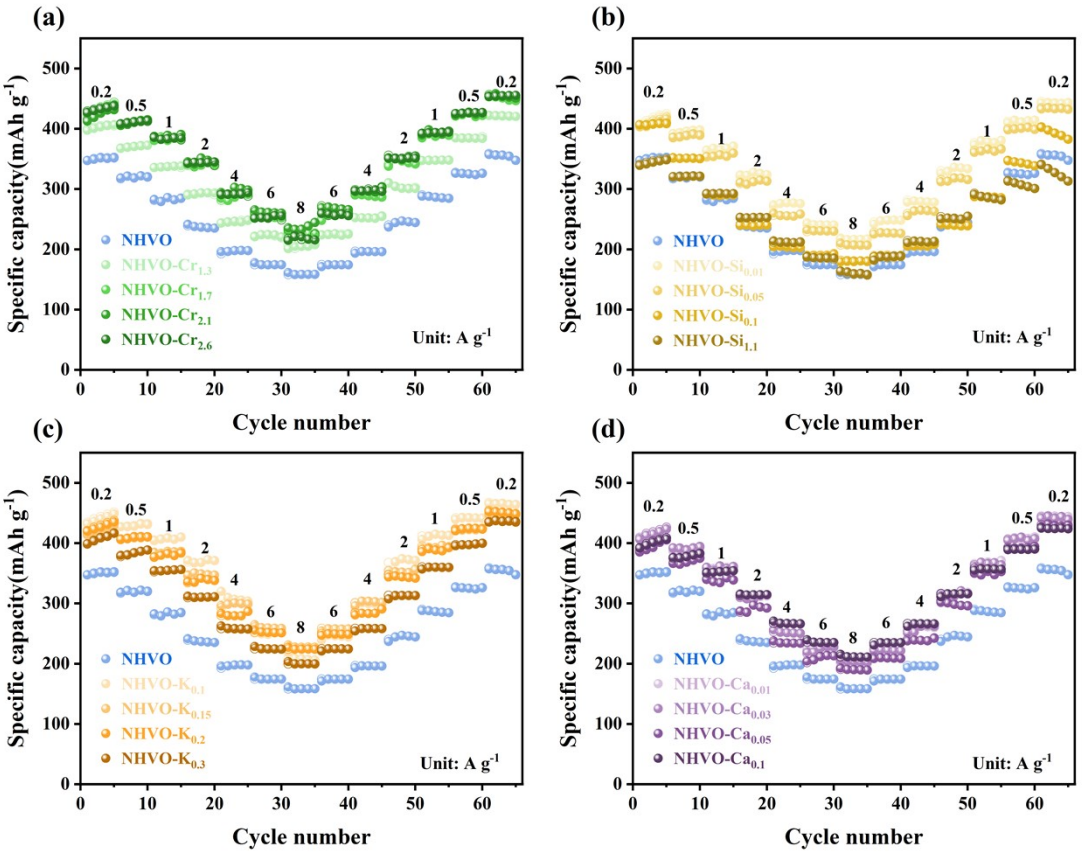

Fig. S2 Rate performance of (a) NHVO-Cr, (b) NHVO-Si, (c) NHVO-Ca, and (d) NHVO-K, synthesized from leachates containing Cr, Si, Ca, and K within actual concentration ranges, respectively, as cathodes for AZIBs.

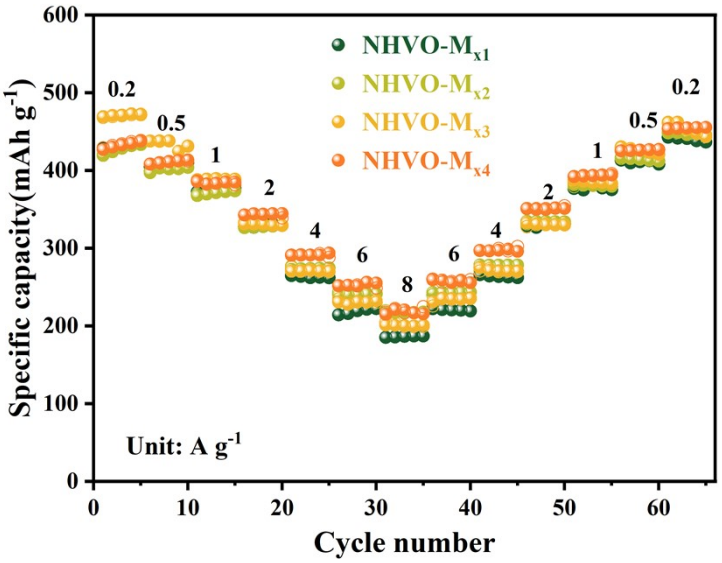

Fig. S3 Rate performance of NHVO-$M_{x\ (1,2,3,4)}$ synthesized from desiliconized leachates containing Cr, Ca, and K of different actual concentration, as cathodes for AZIBs.

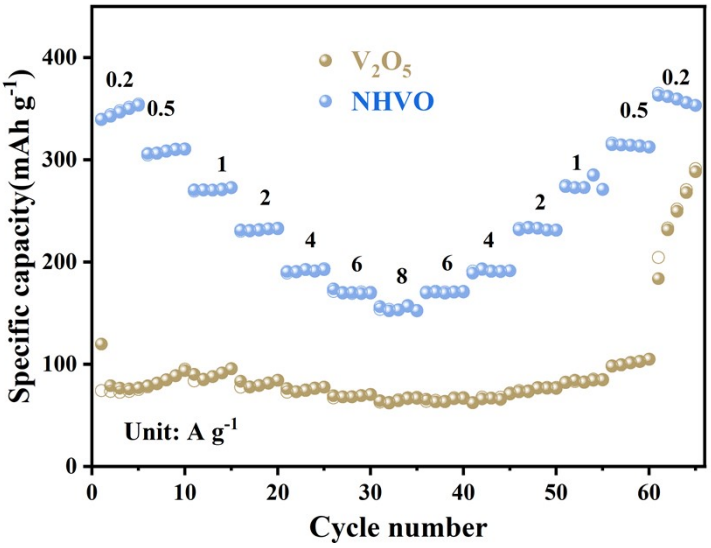

Fig. S4 Comparison of the rate performance between V_2O_5 and NHVO.

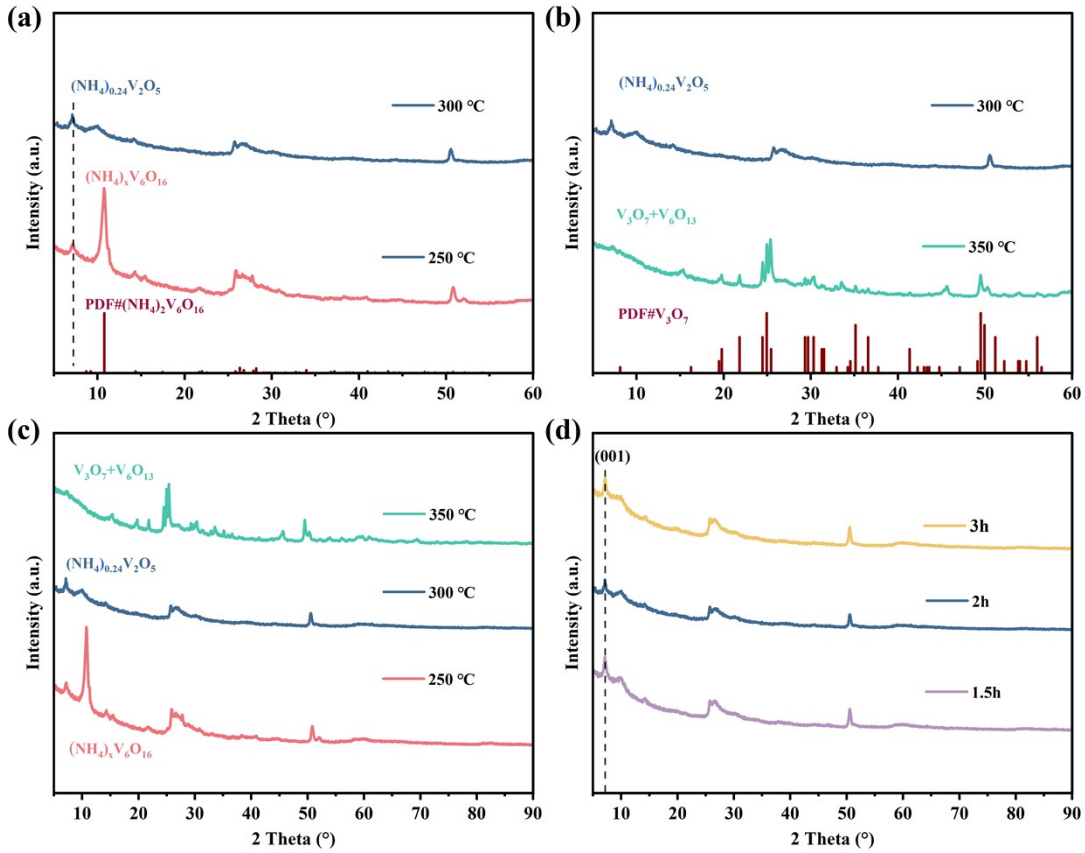

Fig. S5 XRD analysis of vanadium oxides obtained by calcining the precursor in a nitrogen atmosphere at (a) 250 °C and (b) 350°C for 2 h. (c) Comparison of XRD patterns of vanadium oxides at different calcination temperatures. (d) XRD analysis of vanadium oxides obtained by calcining the precursor in a nitrogen atmosphere at 300 °C for 1.5 h, 2 h, and 3 h.

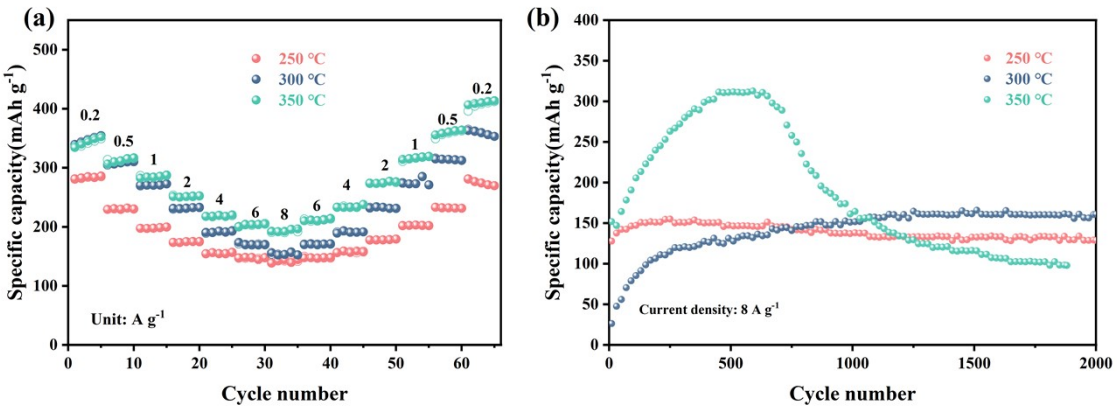

Fig. S6 (a) Rate performance and (b) Cycling performance at 8 A g^{-1} of vanadium oxides obtained at different calcination temperatures under nitrogen atmosphere.

At the initial cycles, a significant increase in capacity occurs due to the activation of the active material.[9] This enhancement in capacity is further strengthened as the ratio of V^{5+} to V^{4+} increases. Additionally, the gradual stabilization of the electrolyte penetration into the interlayer and the increased utilization of the internal active materials also contribute significantly to the substantial improvement in specific capacity.[10]

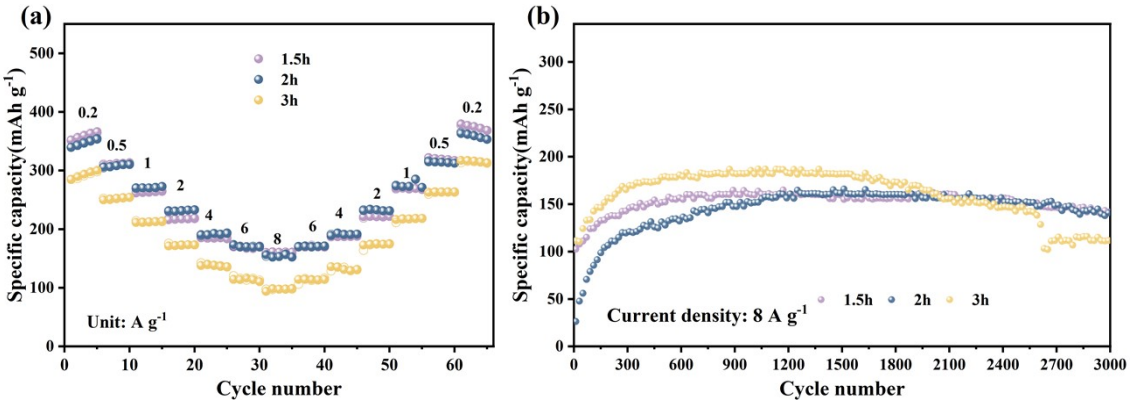

Fig. S7 (a) Rate performance (b) Cycling performance at 8 A g^{-1} of vanadium oxides obtained at different calcination times at 300°C under nitrogen atmosphere.

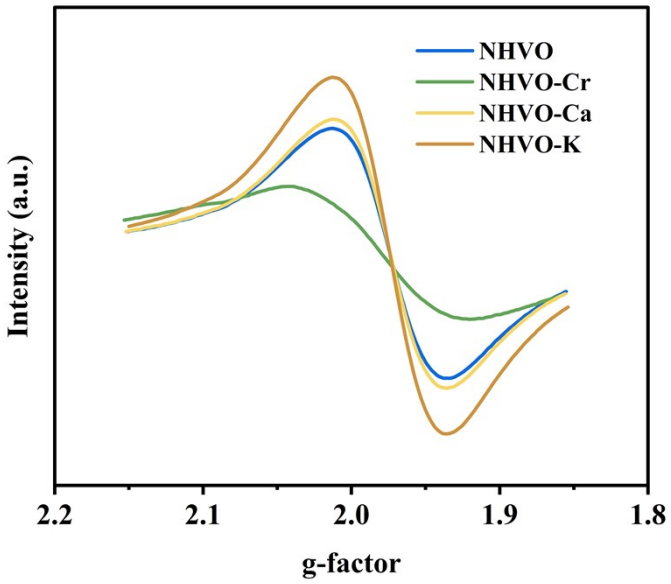

Fig. S8 EPR spectra of NHVO, NHVO-Cr, NHVO-Ca, NHVO-K.

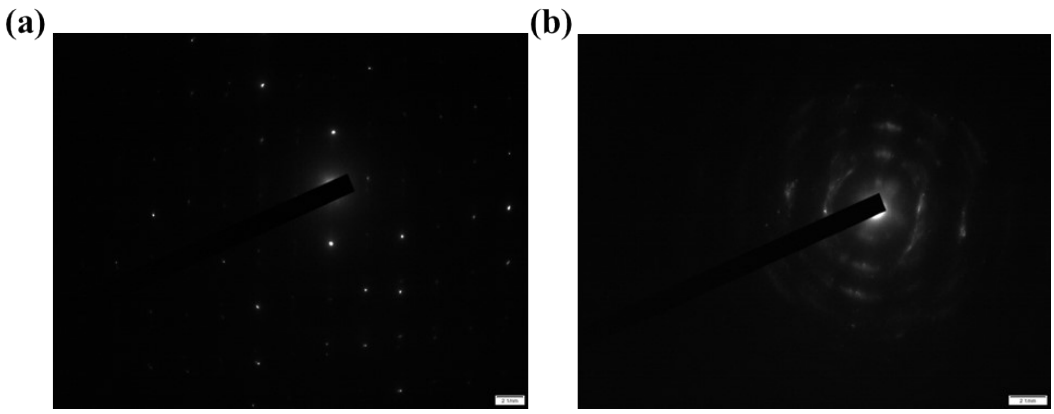

Fig. S9 (a) Selected area electron diffraction (SAED) pattern of V_2O_5 and (b)NHVO-M_x.

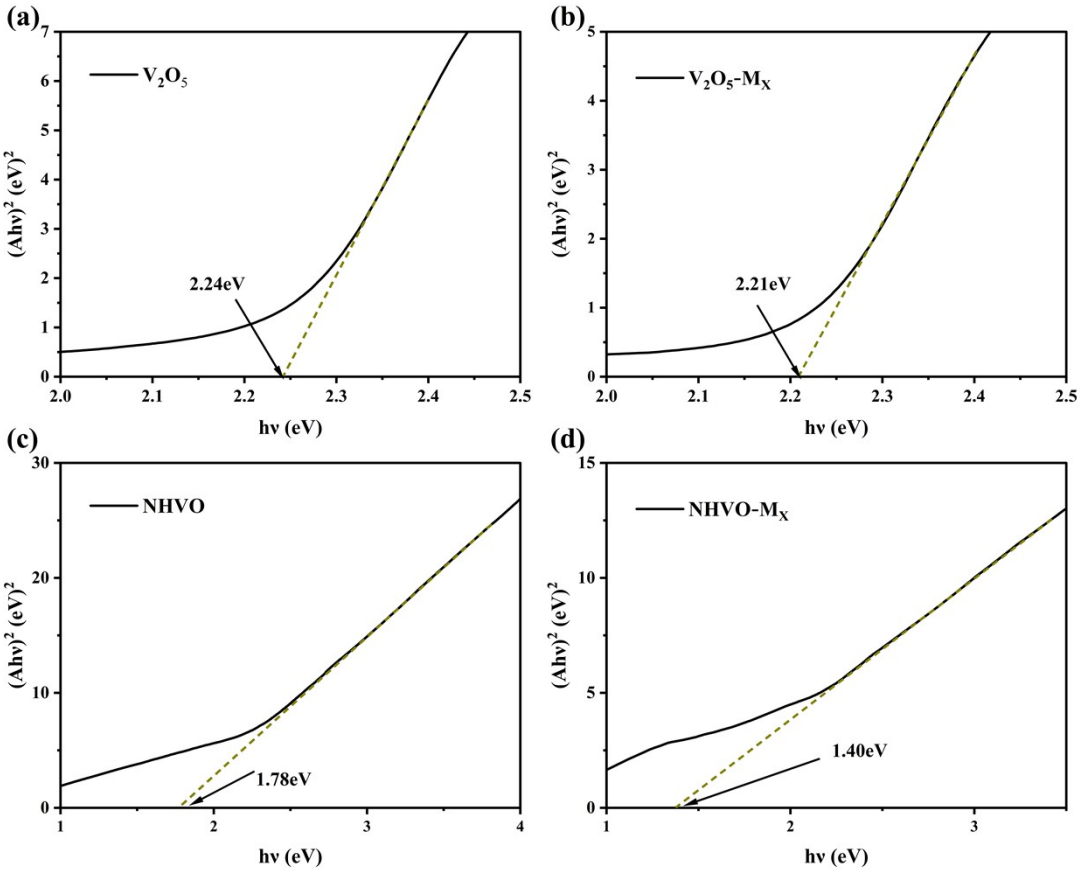

Fig. S10 Band gap of (a) V_2O_5, (b) V_2O_5-M_x, (c) NHVO, and (d) NHVO-M_x obtained from UV-Vis diffuse reflectance spectroscopy (UV-Vis DRS).

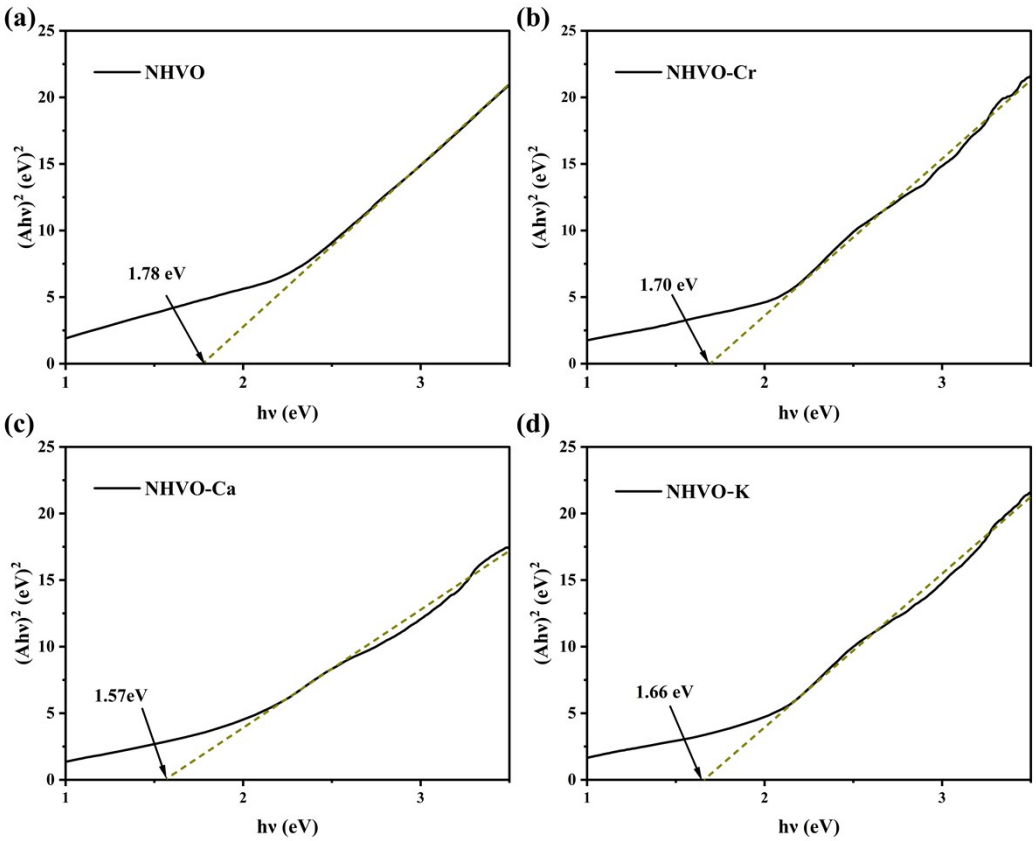

Fig. S11 Band gap of (a) NHVO, (b) NHVO-Cr, (c) NHVO-Ca, and (d) NHVO-K obtained from UV-Vis DRS.

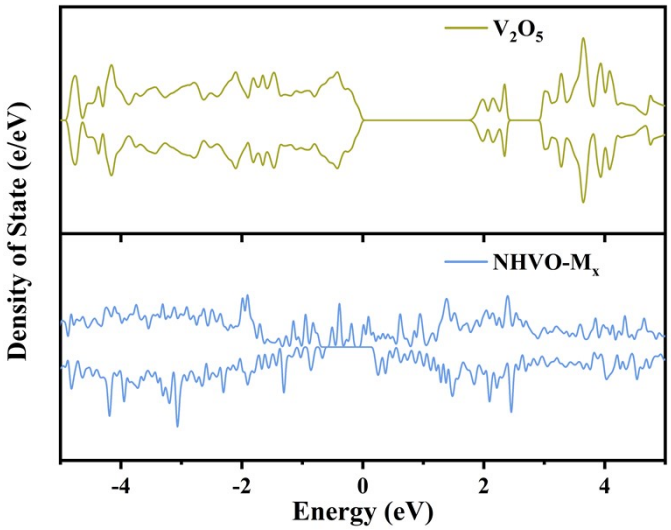

Fig. S12 The density of states (DOS) of V_2O_5 and NHVO-M_x.

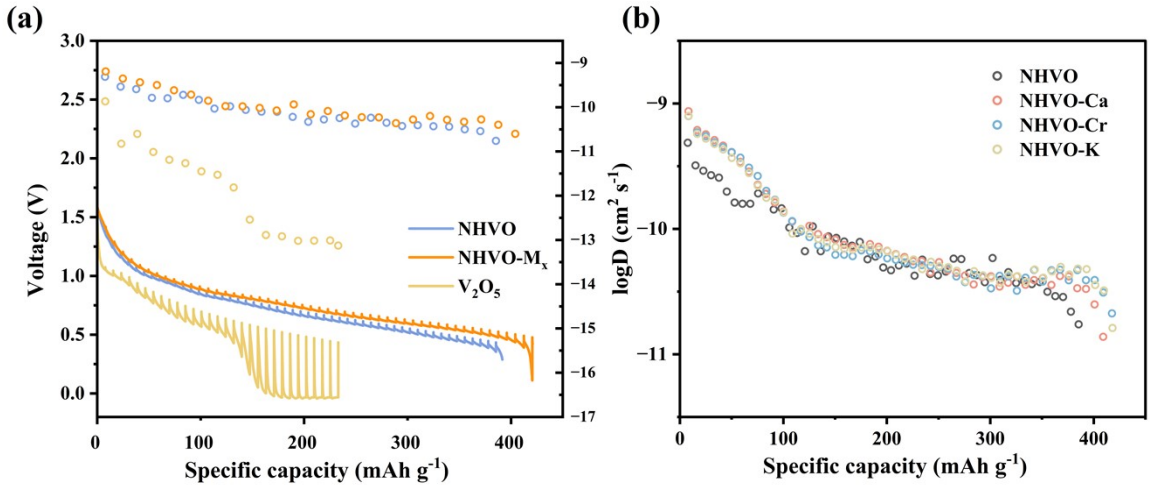

Fig. S13 (a) GITT curves and zinc ion diffusion coefficients of NHVO-M_x, NHVO, and V_2O_5. (b) Zinc ion diffusion coefficients of NHVO-Ca, NHVO-Cr, NHVO-K.

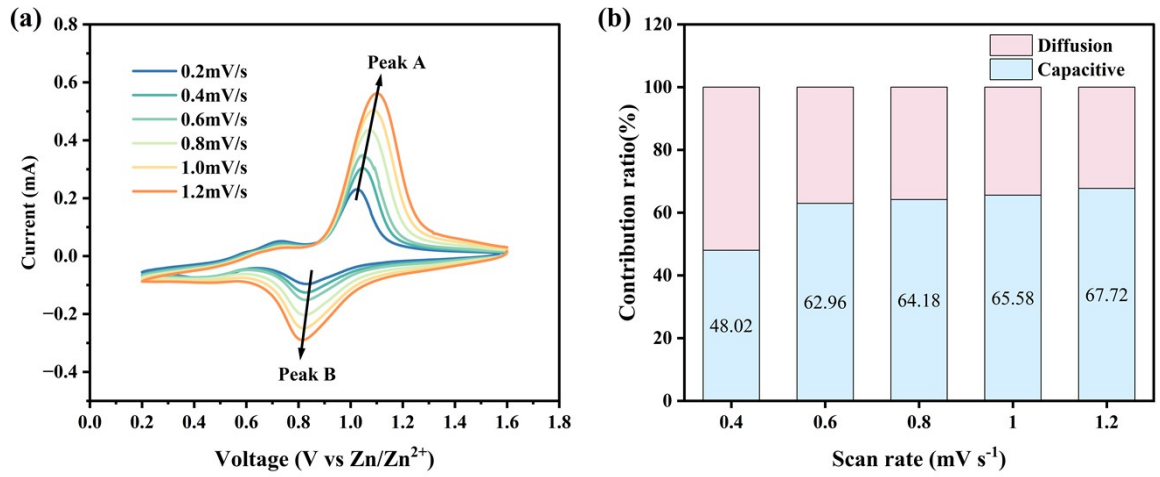

Fig. S14 (a) CV curves of NHVO-Mx at different scan rates. (b) Corresponding capacitive contributions of NHVO-M_x at different scan rates.

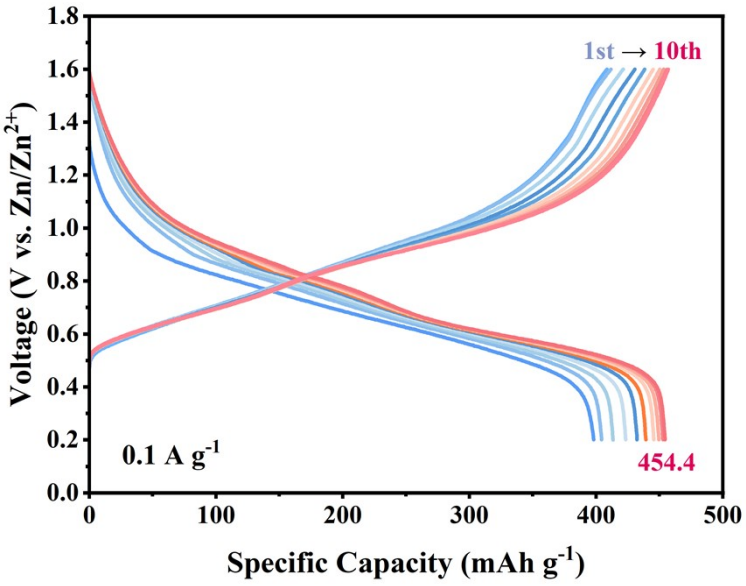

Fig. S15 GCD curves of NHVO-M_x for the first ten cycles at 0.1 A g^{-1}.

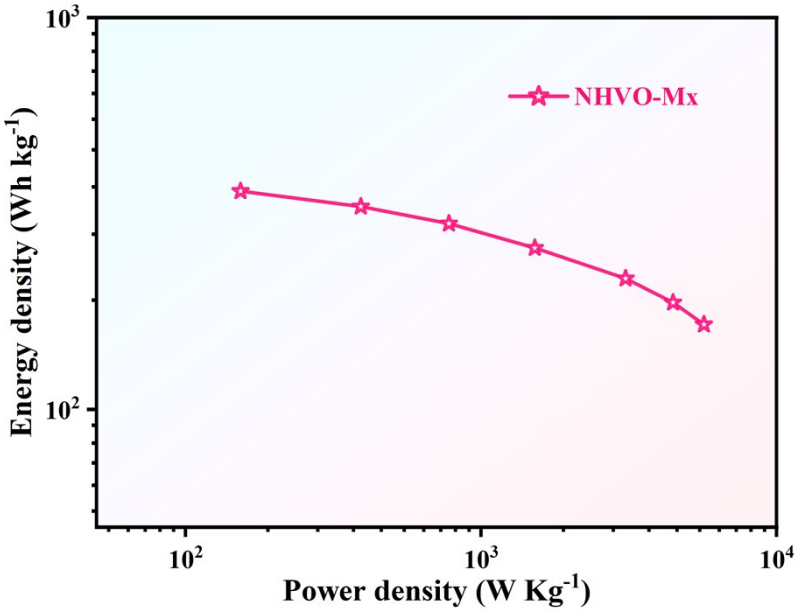

Fig. S16 Ragone plot of NHVO-M_x.

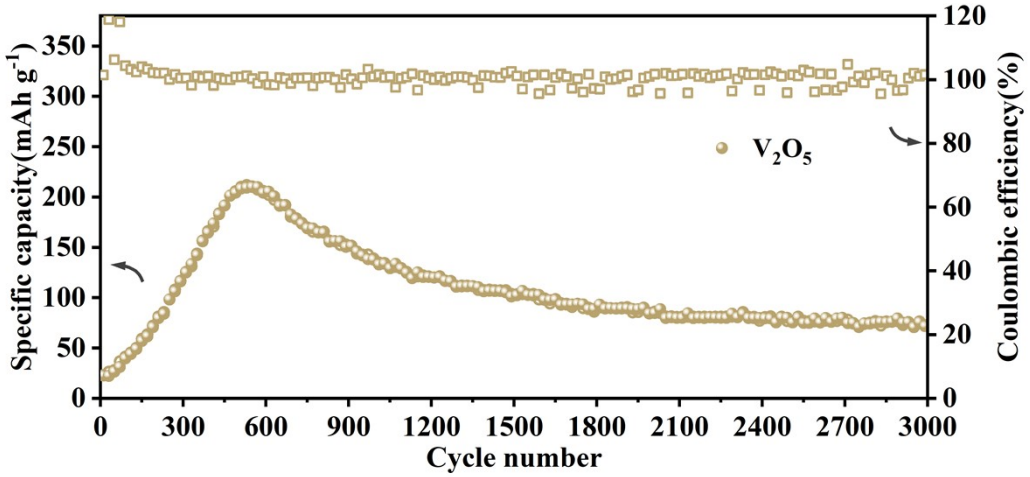

Fig. S17 Cycling performance of V_2O_5 at 8 A g^{-1}.

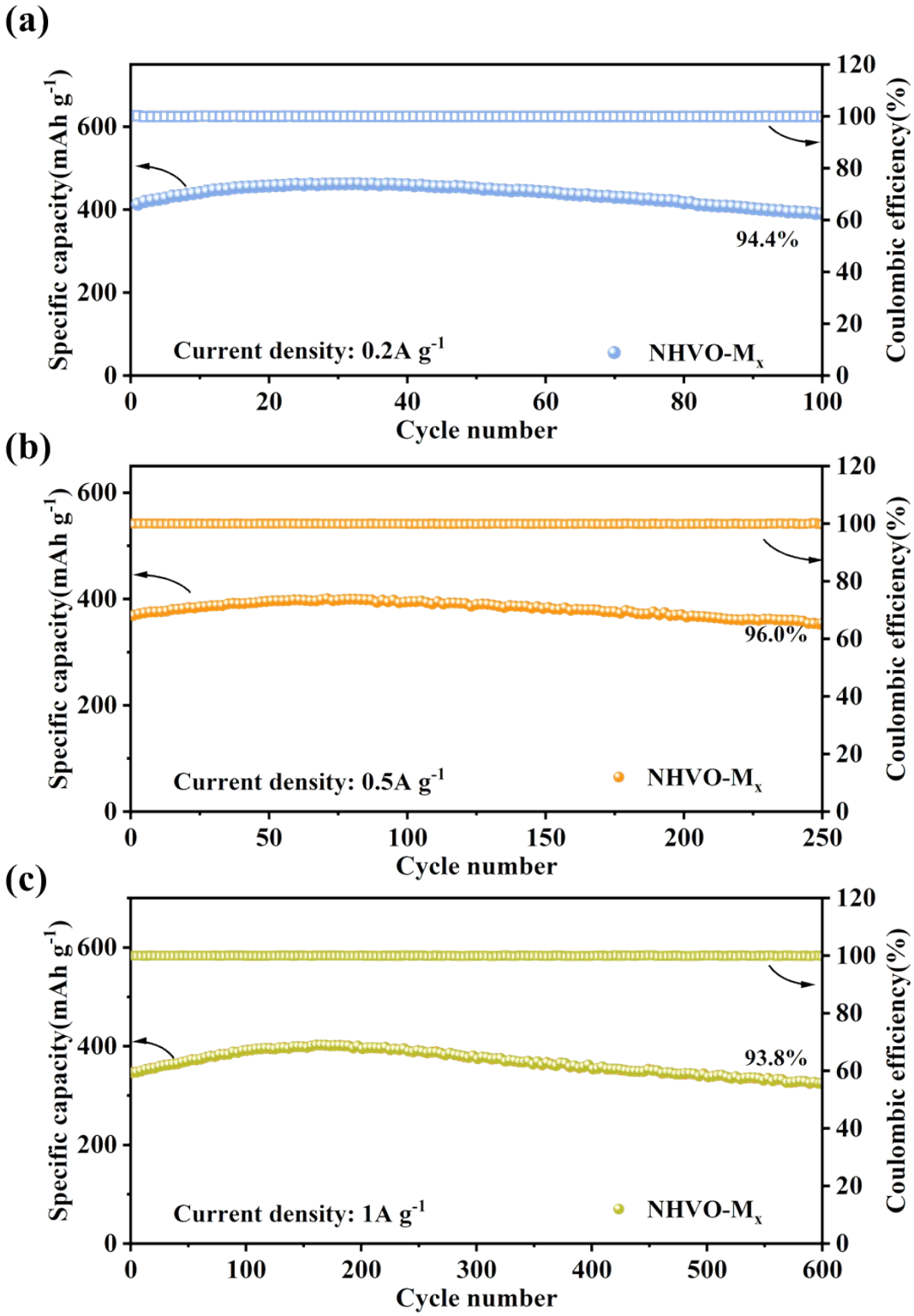

Fig. S18 Cycling stability of NHVO-M_x at (a) 0.2 A g^{-1} (b) 0.5 A g^{-1} and (c) 1 A g^{-1}.

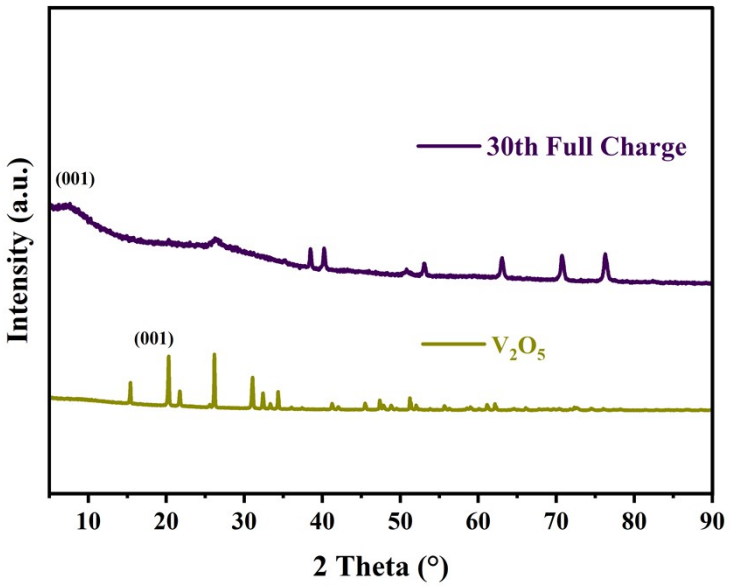

Fig. S19 XRD patterns of V_2O_5 and after 30 cycles of activation at 0.2 A g^{-1}.

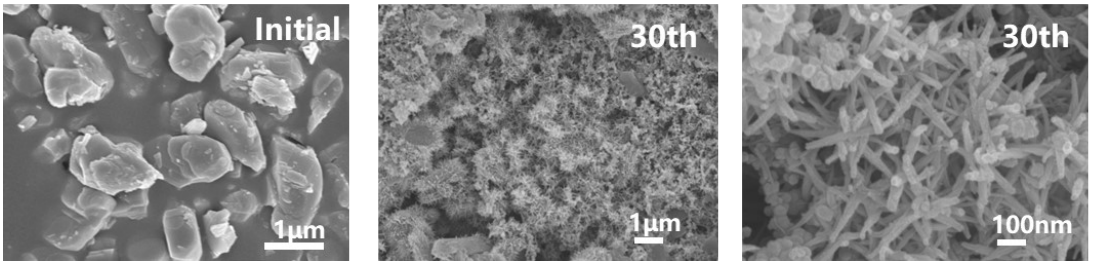

Fig. S20 SEM images of V_2O_5 before and after 30 cycles.

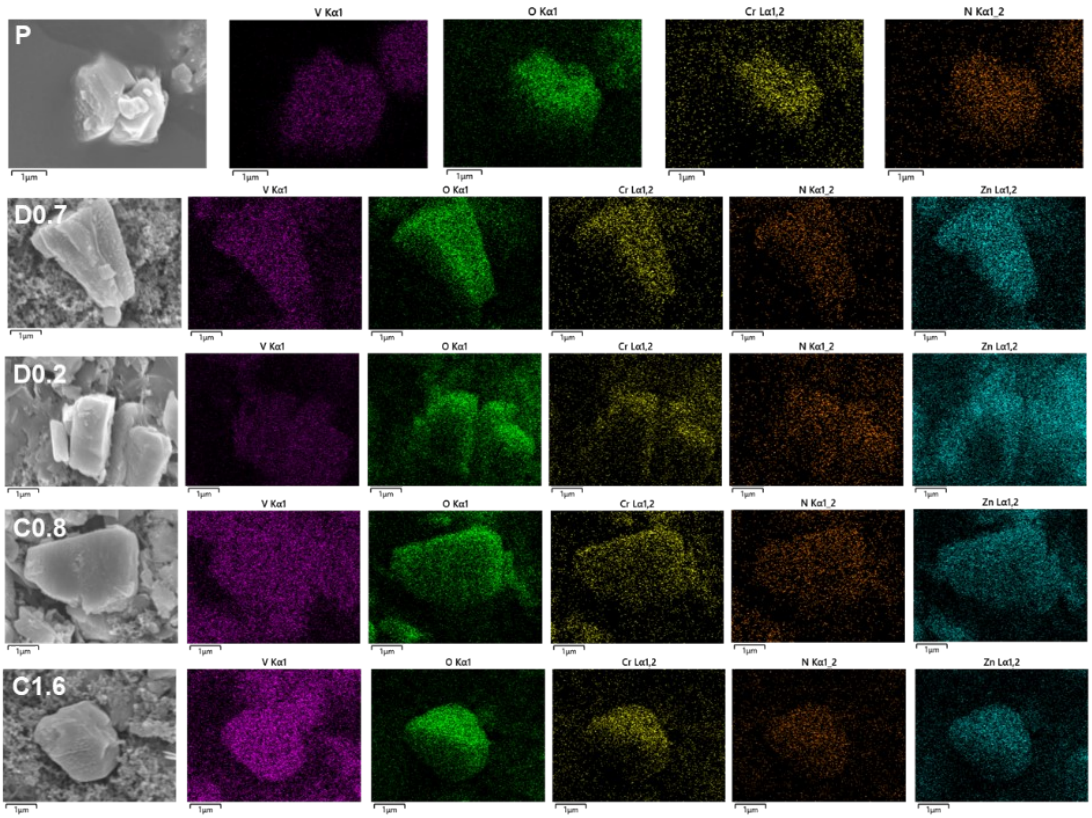

Fig. S21 SEM and EDS images of NHVO-M_x during charge and discharge cycles.

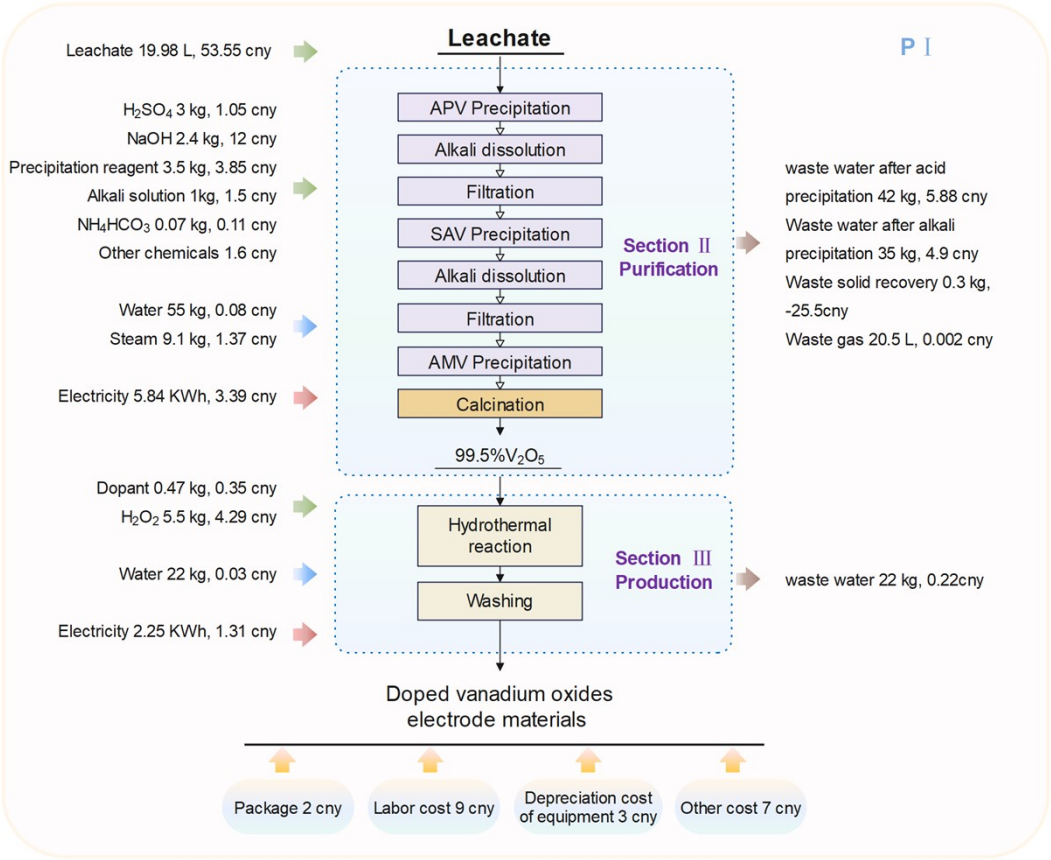

Fig. S22 System boundary of PI.

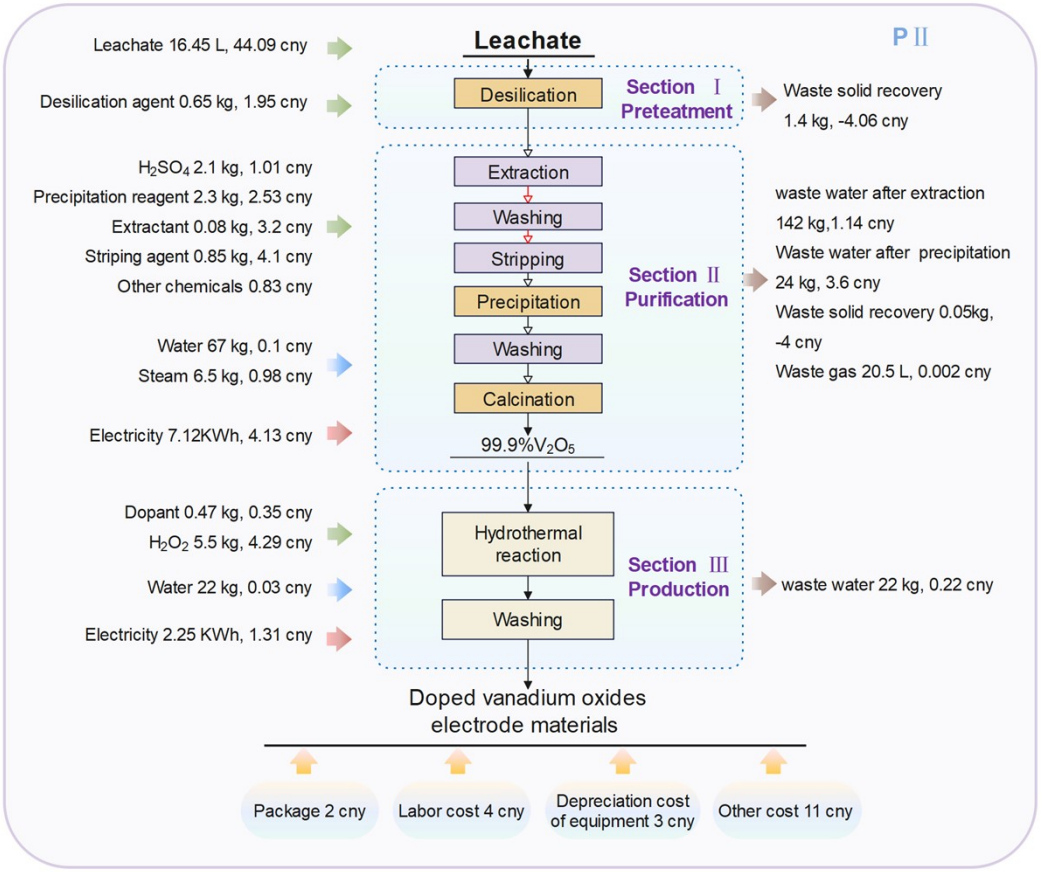

Fig. S23 System boundary of PII.

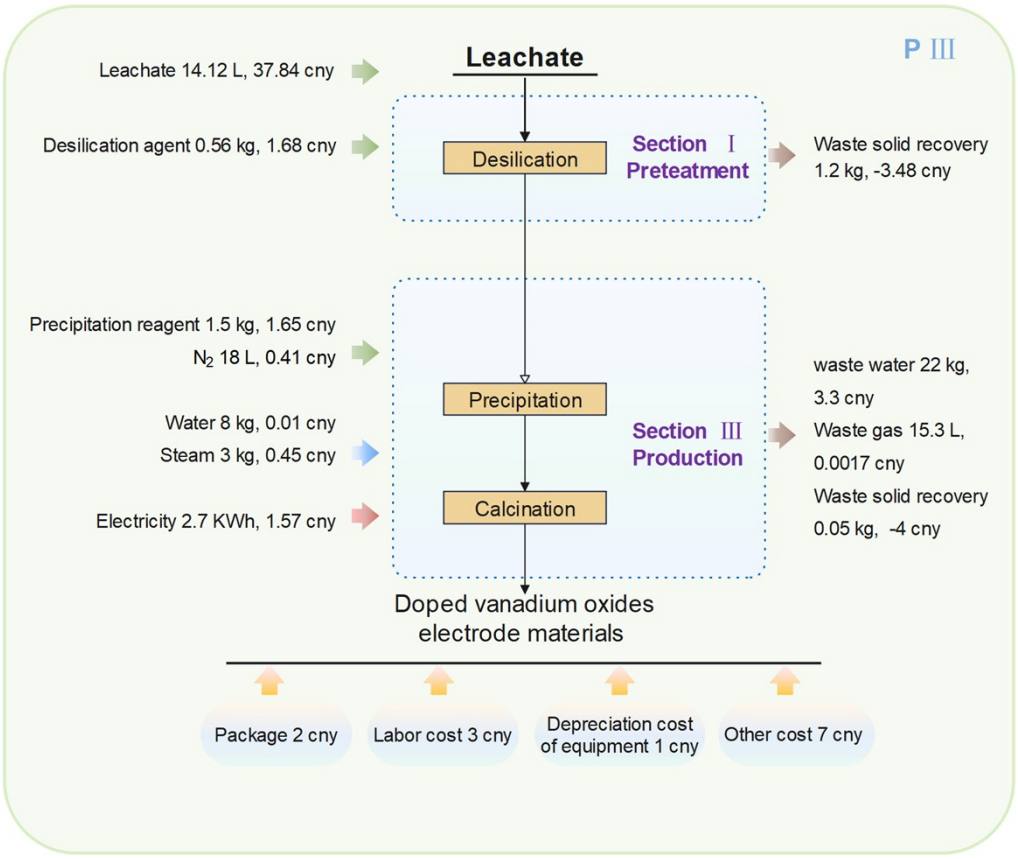

Fig. S24 System boundary of PIII

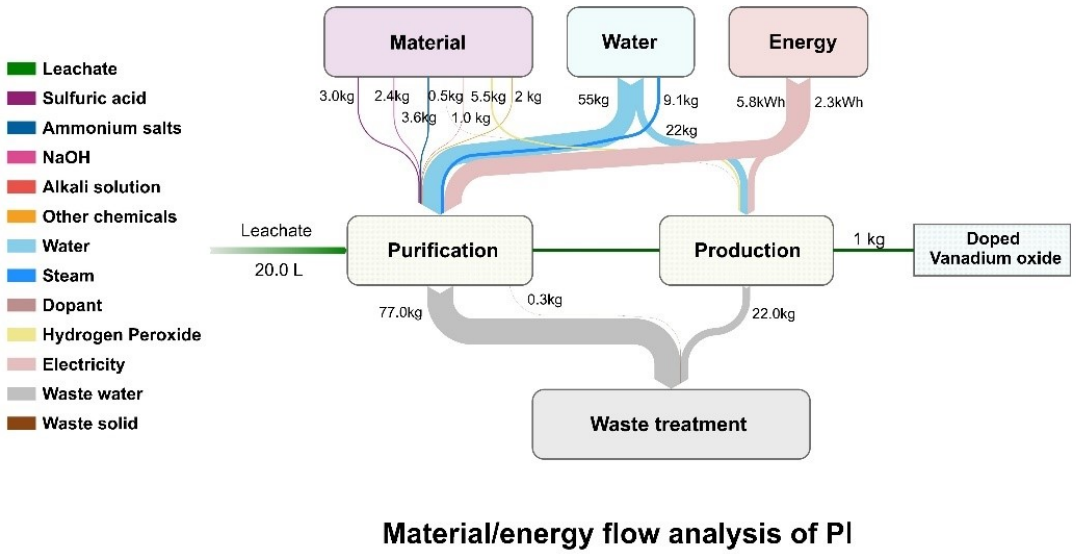

Fig. S25 Material and energy flow of PI.

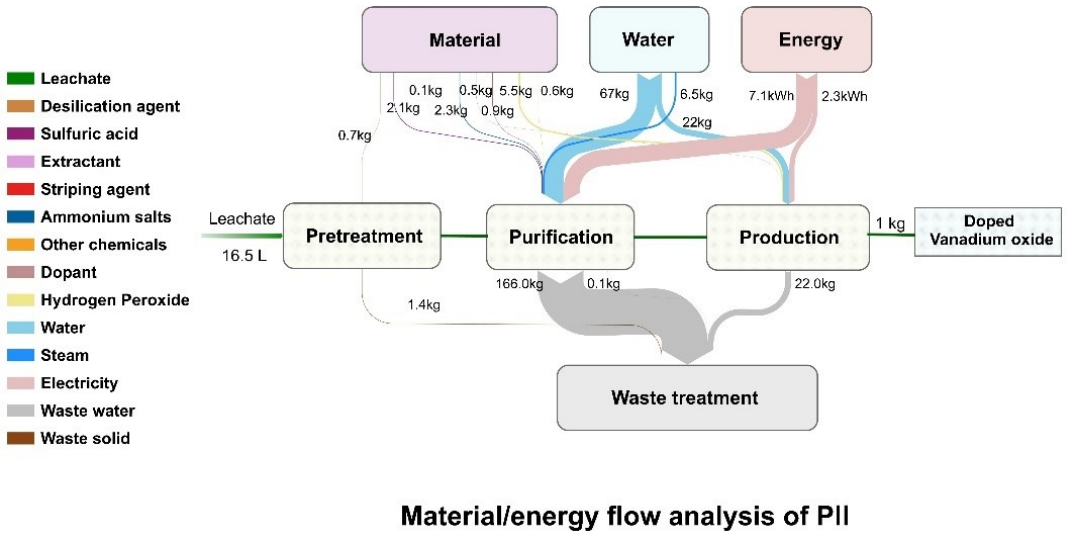

Fig. S26 Material and energy flow of PII.

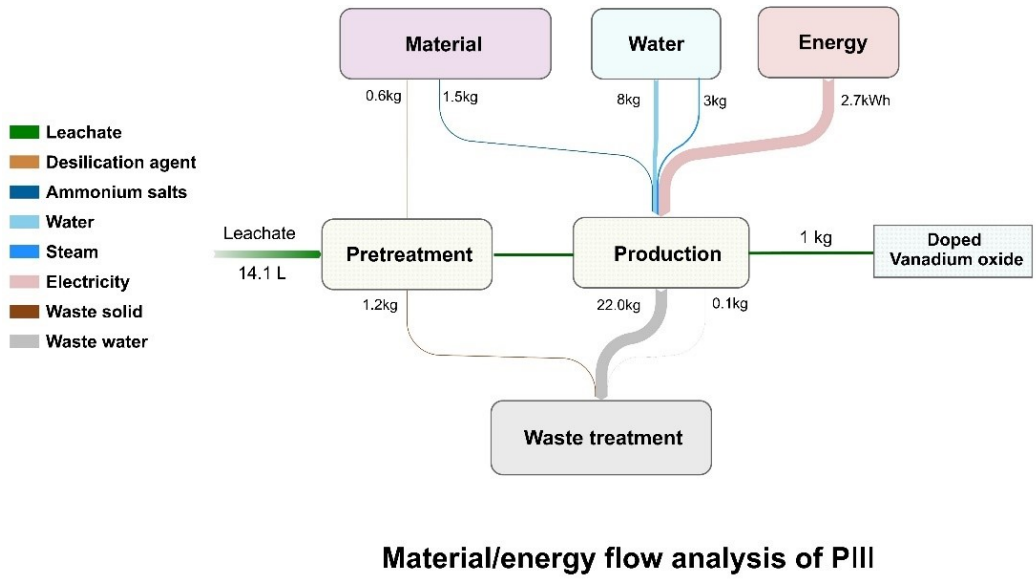

Fig. S27 Material and energy flow of PIII.

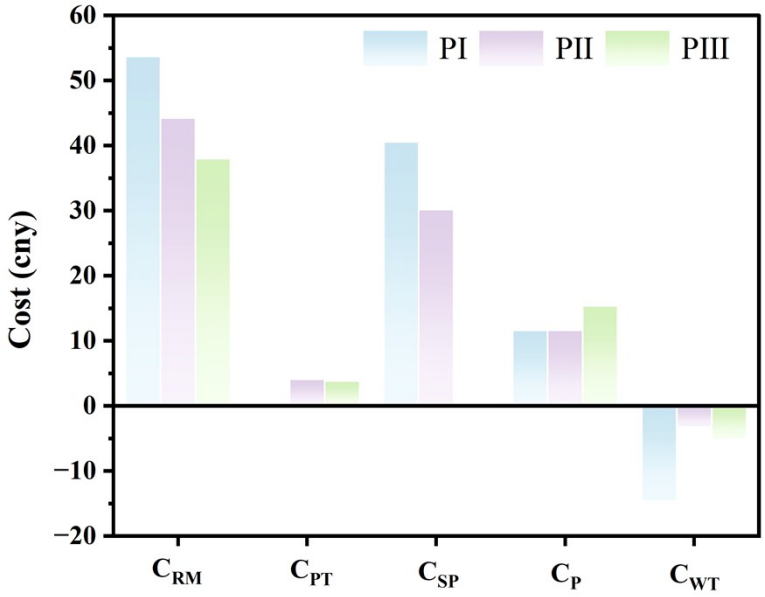

Fig. S28 Comparison of costs at different stages across three production processes.

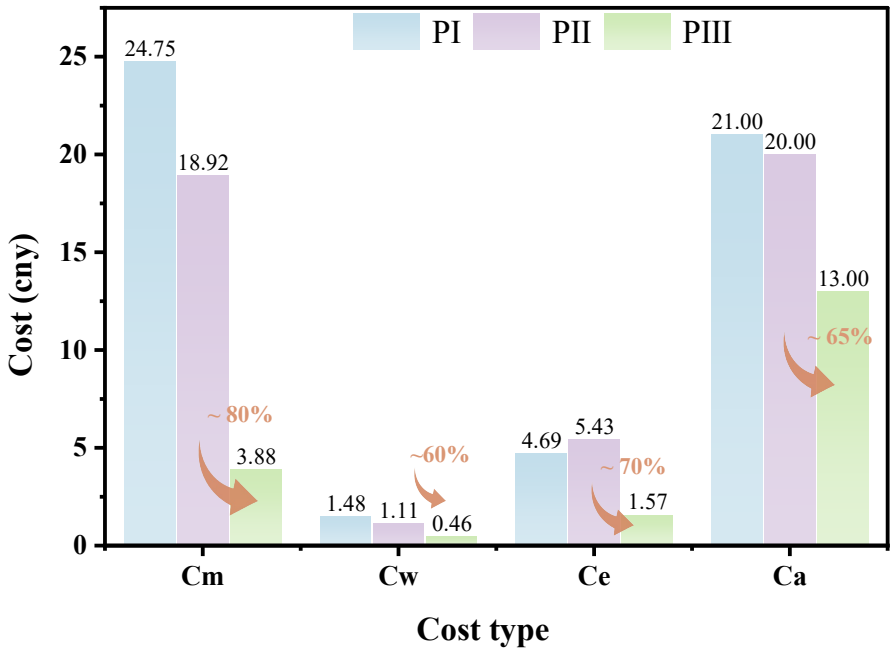

Fig. S29 Costs of different types in the three production processes.

2.2 Supplementary Tables

Table S1. ICP results for the main chemical composition of alkaline leachate from V slag.

V (g L^{-1})	Cr (g L^{-1})	Si (g L^{-1})	Ca (g L^{-1})	K (g L^{-1})
32.1 ~ 45.6	1.3 ~ 2.22	1.1 ~ 1.59	0.012 ~ 0.1	0.1 ~ 0.3
Al (g L^{-1})	**Fe (g L^{-1})**	**Mg (g L^{-1})**	**Ti (g L^{-1})**	**Na (g L^{-1})**
<0.005	<0.005	<0.005	<0.005	32.5 ~ 34.7

Table S2. ICP results of the variation in main elemental content of leachate before and after desiliconization from V slag.

	V (g L^{-1})	Cr (g L^{-1})	Si (mg L^{-1})	Ca (mg L^{-1})
Leachate sample	44.94	2.06	1440	17.75
Desiliconized sample 1	43.55	1.94	10	13
Desiliconized sample 2	43.95	2.03	14	13

Table S3. The concentration of main metal ions in the desiliconized solutions used for the preparation of doped vanadium oxide cathodes.

	V (g L^{-1})	Cr (g L^{-1})	K (g L^{-1})	Ca (g L^{-1})	Si (g L^{-1})
NHVO-M_X	43	1.7	0.2	0.05	<0.02
NHVO-M_{X1}	43	1.3	0.3	0.1	<0.02
NHVO-M_{X2}	43	1.3	0.1	0.02	<0.02
NHVO-M_{X3}	43	1.7	0.3	0.1	<0.02
NHVO-M_{X4}	43	2.2	0.3	0.1	<0.02

Table S4. The specifications for the elemental content in high-purity vanadium pentoxide products. (%)

Cr	K	Na	Ca	Si	Al	Cl	Mg	Mn	Ti
<0.001	0.009	0.006	0.007	0.010	0.001	<0.003	<0.001	<0.001	<0.001

Table S5. The N content and structure of the product of ammonium metavanadate calcined at 300°C for different durations.

Calcination temperature (℃)	Calcination time (h)	N content (mass percentage %)	Crystal structure
300	1.5	1.67%	$(NH_4)_{0.22}V_2O_5$
300	2	1.79%	$(NH_4)_{0.24}V_2O_5$
300	3	1.41%	$(NH_4)_{0.19}V_2O_5$

Table S6. The N content and structure of the product of ammonium metavanadate calcined at different temperatures for 2 h.

Calcination temperature (℃)	Calcination time (h)	N content (mass percentage %)	Crystal structure
250	2	3.31%	$(NH_4)_xV_6O_{16}$+$(NH_4)_yV_2O_5$
300	2	1.79%	$(NH_4)_{0.24}V_2O_5$
350	2	0.25%	$(NH_4)_x$-V_3O_7+V_6O_{13}

Table S7. Cost calculation of PI process

Cost item	Unit	Unit cost (cny)	Raw data	Cost (cny)
1.Main raw material				**53.5464**
Leachate (vanadium, 40 g/L)	L	2.68	19.98	53.5464
2.Auxiliary materials				**24.7475**
H_2SO_4	kg	0.35	3	1.05
NaOH	kg	5	2.4	12
Precipitation reagent	kg	1.1	3.5	3.85
Alkali solution	kg	1.5	1	1.5
NH_4HCO_3	kg	1.5	0.07	0.105
Dopant	kg	0.75	0.47	0.3525
H_2O_2-30%	kg	0.78	5.5	4.29
Other materials				1.6
3.Package				**2**
4.Waste treatment				**-14.497745**
Waste water after acid precipitation	kg	0.14	42	5.88
Waste water after alkali precipitation	kg	0.14	35	4.9
Waste water after hydrothermal reaction	kg	0.01	22	0.22
Waste solid recovery	kg	85	-0.3	-25.5
Waste gas	L	0.00011	20.5	0.002255
5.Fuel and power				**6.1727**
Water	kg	0.0015	77	0.1155
Electricity	kW·h	0.58	8.09	4.6922
Steam	kg	0.15	9.1	1.365
Total cost of material consumption				**71.968855**
6.Other costs				**19**
Labor cost				9
Depreciation cost of equipment				3
Variable cost				2
Period cost				5
Total cost				**90.968855**

Table S8. Cost calculation of PII process

Cost item	Unit	Unit cost (cny)	Raw data	Cost (cny)
1.Main raw material				**44.086**
Leachate (vanadium,40 g/L)	L	2.68	16.45	44.086
2.Auxiliary materials				**18.9205**
Desilication agent	kg	3	0.65	1.95
Extractant	kg	40	0.08	3.2
Striping agent	kg	5.6	0.85	4.76
Precipitation reagent	kg	1.1	2.3	2.53
H_2SO_4-98%	kg	0.48	2.1	1.008
Aluminum sulfate	kg	0.75	0.47	0.3525
H_2O_2-30%	kg	0.78	5.5	4.29
Other materials				0.83
3.Package				**2**
4.Waste treatment				**-3.101745**
Waste water after extraction	kg	0.008	142	1.136
Waste water after vanadium precipitation	kg	0.15	24	3.6
Waste water after hydrothermal reaction	kg	0.01	22	0.22
Waste solid recovery-after desilication	kg	2.9	-1.4	-4.06
Waste solid recovery after calcination	kg	80	-0.05	-4
Waste gas	L	0.00011	20.5	0.002255
5.Fuel and power				**6.5431**
Water	kg	0.0015	89	0.1335
Electricity	kW·h	0.58	9.37	5.4346
Steam	kg	0.15	6.5	0.975
Total cost of material consumption				**68.447855**
6.Other costs				**18**
Labor cost				4
Depreciation cost of equipment				3
Variable cost				6
Period cost				5
Total cost				**86.447855**

Table S9. Cost calculation of PIII process

Cost item	Unit	Unit cost (cny)	Raw data	Cost (cny)
1.Main raw material				**37.8416**
Leachate (vanadium, 40 g/L)	L	2.68	14.12	37.8416
2.Auxiliary materials				**3.882**
Desilication agent	kg	3	0.56	1.68
Precipitation reagent	kg	1.1	1.5	1.65
N_2	L	0.023	24	0.552
3.Package				**2**
4.Waste treatment				**-4.92571**
Waste water-after vanadium precipitation	kg	0.15	17	2.55
Waste solid recovery-after desilication	kg	2.9	-1.2	-3.48
Waste solid recovery-after calcination	kg	80	-0.05	-4
Waste gas	L	0.00011	39	0.00429
5.Fuel and power				**2.028**
Water	kg	0.0015	8	0.012
Electricity	kW·h	0.58	2.7	1.566
Steam	kg	0.15	3	0.45
Total cost of material consumption				**40.82589**
6.Other costs				**11**
Labor cost				3
Depreciation cost of equipment				1
Variable cost				2
Period cost				5
Total cost				**51.82589**

Table S10. Comprehensive environmental assessment of PI process

PI	Waste type	$S_{max,x,y}$ mg/L	S_x* mg/L	R_x	W_x	CEA	TCEA
Waste water (mg/L)	V	1.00E+02	2.00E+00	5.00E+01	7.11E-02	2.93E+00	1.26E+03
	Cr	2.00E+02	5.00E-01	4.00E+02	5.69E-01	4.76E+01	
	NH_4^+-N	5.40E+03	2.50E+01	2.16E+02	3.07E-01	6.93E+02	
	SO_4^{2-}	3.00E+04	1.00E+03	3.00E+01	4.26E-02	5.19E+02	
	SiO_2	3.00E+02	5.00E+01	6.00E+00	8.53E-03	8.96E-01	
	SS	1.00E+02	7.00E+01	1.43E+00	2.03E-03	2.56E-02	
Waste gas (mg/m^3)	Particulates	2.13E+02	1.00E+02	2.13E+00	1.00E+00	2.32E+00	2.32E+00
Waste solid (Kg)						0.00E+00	0.00E+00
Total value							1.27E+03

Table S11. Comprehensive environmental assessment of PII process

PII	Waste type	$S_{max,x,y}$ mg/L	S_x* mg/L	R_x	W_x	CEA	TCEA
Waste water (mg/L)	V	1.22E+02	2.00E+00	6.10E+01	8.67E-02	7.91E+00	5.88E+02
	Cr	1.33E+03	5.00E-01	2.65E+03	3.77E+00	4.99E+02	
	COD_{Cr}	1.37E+03	3.00E+01	4.56E+01	6.48E-02	6.58E+01	
	NH_4^+-N	1.47E+02	2.50E+01	5.86E+00	8.34E-03	7.70E-01	
	SO_4^{2-}	3.48E+03	1.00E+03	3.48E+00	4.94E-03	9.29E+00	
	Oil	2.20E+02	1.00E+01	2.20E+01	3.13E-02	4.99E+00	
Waste gas (mg/m^3)	Particulates	2.13E+02	1.00E+02	2.13E+00	1.00E+00	2.32E+00	2.32E+00
Waste solid (Kg)						0.00E+00	0.00E+00
Total value							5.90E+02

Table S12. Comprehensive environmental assessment of PIII process

PII	Waste type	$S_{max,x,y}$ mg/L	S_x* mg/L	R_x	W_x	CEA	TCEA
Waste water (mg/L)						0.00E+00	0.00E+00
Waste gas (mg/m^3)	Particulates	2.13E+02	1.00E+02	2.13E+00	1.00E+00	4.41E+00	4.41E+00
Waste solid (Kg)						0.00E+00	0.00E+00
			Total value				4.41E+00

References

1 T. D. Kühne, M. Iannuzzi, M. Del Ben, V. V. Rybkin, P. Seewald, F. Stein, T. Laino, R. Z. Khaliullin, O. Schütt, F. Schiffmann, D. Golze, J. Wilhelm, S. Chulkov, M. H. Bani-Hashemian, V. Weber, U. Borštnik, M. Taillefumier, A. S. Jakobovits, A. Lazzaro, H. Pabst, T. Müller, R. Schade, M. Guidon, S. Andermatt, N. Holmberg, G. K. Schenter, A. Hehn, A. Bussy, F. Belleflamme, G. Tabacchi, A. Glöß, M. Lass, I. Bethune, C. J. Mundy, C. Plessl, M. Watkins, J. VandeVondele, M. Krack and J. Hutter, *J. Chem. Phys.*, 2020, **152**, 194103.

2 J. VandeVondele, M. Krack, F. Mohamed, M. Parrinello, T. Chassaing and J. Hutter, *Comput. Phys. Commun.*, 2005, **167**, 103–128.

3 C. Hartwigsen, *Phys. Rev. B*, 1998, **58**, 3641–3662.

4 J. P. Perdew, *Phys. Rev. Lett.*, 1996, **77**, 3865–3868.

5 S. Grimme, S. Ehrlich and L. Goerigk, *J. Comput. Chem*, 2011, **32**, 1456–1465.

6 T. Lu and F. Chen, *J. Comput. Chem*, 2012, **33**, 580–592.

7 G. Zhang, Y. Wang, X. Meng, D. Zhang, N. Ding, Z. Ren, W. Gao and Z. Sun, *Resour. Conserv. Recycl.*, 2023, **192**, 106926.

8 W. Gao, Z. Sun, H. Cao, H. Ding, Y. Zeng, P. Ning, G. Xu and Y. Zhang, *J. Cleaner Prod.*, 2020, **256**, 120217.

9 X. Liang, L. Yan, W. Li, Y. Bai, C. Zhu, Y. Qiang, B. Xiong, B. Xiang and X. Zou, *Nano Energy*, 2021, **87**, 106164.

10 J. He, X. Liu, H. Zhang, Z. Yang, X. Shi, Q. Liu and X. Lu, *ChemSusChem*, 2020, **13**, 1568–1574.